



21.83% incident light can circumvent a 6.6×6.6 cm² obstruction by introducing a layer of bubbles into the photovoltaic glass

YINGFENG LI,^{1,3}  JIAYUAN AN,¹ YONGSHUAI GONG,²
CHAO WANG,¹ DONGXUE LIU,² ZHIHAN LIU,¹ WENXIANG GAO,¹
YINGJIAN LIU,¹ AND MEICHENG LI^{1,4} 

¹State Key Laboratory of Alternate Electrical Power System with Renewable Energy Sources, North China Electric Power University, Beijing 102206, China

²Three Gorges Corporation, Institute of Science and Technology, Beijing 100038, China

³liyinfeng@ncepu.edu.cn

⁴mcli@ncepu.edu.cn

Abstract: Obstruction is inevitable and will significantly impact the actual output performance of photovoltaic modules, even jeopardize their operational safety. We introduced a layer of bubbles into photovoltaic glass. These bubbles can alter the path of incident light, while the internal reflection at the glass/air interface enables the redirected light rays to have longer lateral propagation distance, circumventing the obstructions. The optimized photovoltaic glass with a bubble diameter of 1.8 mm and a surface density of 16 cm⁻² enables the light intensity underneath a 6.6×6.6 cm² obstruction to reach 21.83% of the incident light intensity. This enhancement permits a partial shading of the photovoltaic module, increasing its output power by ~20.8% and decreasing the reverse bias voltage on the shaded cell by ~1.4 V.

© 2024 Optica Publishing Group under the terms of the [Optica Open Access Publishing Agreement](#)

1. Introduction

In the context of global energy transition, photovoltaic power generation has garnered significant attention as a clean and highly efficient electricity generation technology. During the actual operation of photovoltaic modules, they are inevitably subjected to shading from surrounding structures [1], cloud cover [2,3], vegetation such as trees and leaves, as well as dust accumulation [4]. Consequently, photovoltaic modules inevitably operate in partial shade conditions [5,6].

In most photovoltaic modules, the solar cells are interconnected in series and parallel. When one or several cells are shaded, the shaded cells' power output diminishes, causing a mismatch among different cells within the module [7]. This mismatching adversely impacts the overall performance of the module due to series-parallel effects [8–10]. Furthermore, this shading can lead to the shaded cells acting as a load within the module [11,12], operating in a reverse-biased state, thereby generating hotspots [13,14]. This will significantly impact the lifespan of the photovoltaic module [15,16], and in certain cases, the reverse bias voltage may even reach the reverse breakdown voltage of the solar cells [17,18], potentially damaging the photovoltaic module and posing safety risks [19]. Therefore, conducting research aimed at enhancing the power generation of photovoltaic modules under shading conditions and mitigating hotspot formation is of paramount importance.

If the irradiance received by shaded cells can be increased, it offers two advantages. On one hand, it can enhance the shaded cells' photocurrent, thus reducing mismatch with other cells. For example, supposing one cell in a 72×2 series-parallel connected photovoltaic module (e.g., the Deep Blue 3.0 JAM72S30 530-555/MR modules of JA solar) is completely shaded, the module's output power will be reduced to 50% compared to an unshaded scenario. However, if the shaded cell can receive 10% of the incident light intensity, the module's output power can reach 55%

compared to the unshaded condition. On the other hand, it can also decrease the reverse bias voltage on the shaded cell, lowering hotspot temperature and consequently safeguarding the photovoltaic module. This work aims to design a type of photovoltaic glass that allows some incident light to “circumvent” obstructions on it and reach the shaded cells, intending to enhance the output power of the photovoltaic module and reduce hotspot temperatures.

As of now, there have been numerous designs developed for photovoltaic glass. For instance, Park et al. have designed a micro-scale periodic honeycomb texture on the surface of photovoltaic glass, achieving a haze of 52% and a reflectance of 5.74% [20]. Chen et al. have fabricated a regular pit array on the surface of photovoltaic glass, which can reduce the reflectance by 31.91% for thin-film solar cells [21]. Song et al. have proposed a broadband anti-reflective cover glass used in concentrated photovoltaics with moth-eye structures on its surface [22]. Kim et al. have designed a nano-patterned photovoltaic glass that can enhance the absorption of sunlight by silicon solar cells across a wide range of incident angles, 0-60° [23]. Tsai et al. have developed embedded biomimetic nanostructures on a glass substrate, demonstrating broadband-enhanced anti-reflective and light-capturing properties, resulting in increased short-circuit current density for thin-film solar cells [24]. The main objective of these studies is to enhance the haze of the photovoltaic glass, thereby reducing the reflectance of thin-film solar cells [25]. However, none of them focused on the ability of the designed photovoltaic glass to allow incident light to circumvent the obstruction placed upon it.

In this work, we have designed a photovoltaic glass by introducing a layer of bubbles into it. The bubbles can alter the path of incident light, thereby increasing the haze of the glass. Meanwhile, the internal reflection at the glass/air interface enables these redirected light rays to have a long lateral propagation distance, allowing them to circumvent obstruction. Based on ray-tracing simulations, we investigated how the distribution, size, and surface density of bubbles affect the haze of the photovoltaic glass, as well as its ability to allow incident light to circumvent a $6.6 \times 6.6 \text{ cm}^2$ obstruction placed upon it. Subsequently, based on device simulations, we evaluated the efficacy of this photovoltaic glass in enhancing the module’s power output and reducing the reverse bias on the shaded cell. This study provides a novel approach to improve the photovoltaic module’s output power under shadings and suppress hotspot occurrences, holding significant theoretical significance and practical value.

2. Model and method

2.1. Design of the bubble-containing photovoltaic glass

Firstly, we conducted a theoretical analysis of the light path when it irradiates photovoltaic glass containing bubbles. Various scenarios when a single ray of light irradiates a single bubble are depicted in Fig. 1(a). Here, the refractive indices of air and glass, denoted as n_1 and n_2 , are set to 1.0 and 1.46, respectively. According to Snell’s law, the optical total reflection critical angle at the glass/air interface can be calculated as 43°. As shown in the middle diagram of Fig. 1(a), the angle of incidence at the glass/bubble interface is equal to the angle corresponding to the incidence point, denoted as ϕ .

When the incident light strikes the top area of the bubble ($\phi < 43^\circ$), it undergoes multiple reflections and refractions within the bubble. When $43^\circ < \phi < 68.5^\circ$, the light is totally internally reflected at the glass/air interface and does not enter the bubble (as illustrated in the left diagram of Fig. 1(a)); moreover, the light reaching the bottom surface of the glass is again internally reflected at the glass/air interface. However, when $\phi > 68.5^\circ$, the light totally reflected by the bubble has an angle of incidence on the bottom surface of the glass that is less than 43° (as illustrated in the right diagram of Fig. 1(c)); hence, partial light can transmit through the bottom surface of the glass.

Comprehensively, when the light penetrates photovoltaic glass containing bubbles, the path of incident light undergoes significant alterations, thereby potentially enhancing the haze of the

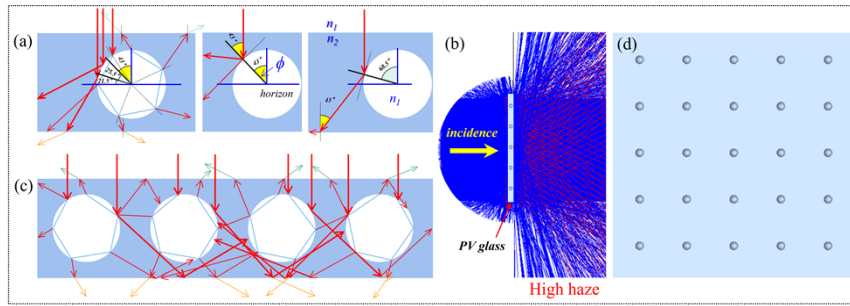


Fig. 1. Schematic of the design principle of photovoltaic glass. (a) light path diagram when a single beam irradiates a single bubble; (b) Illustrative diagram of high-haze photovoltaic glass; (c) path of light within bubble-containing photovoltaic glass; (d) bubble-containing photovoltaic glass.

glass, as illustrated in Fig. 1(b). Simultaneously, the internal reflection at the glass/air interface enables can confine some incident light within the glass, ensuring this type of photovoltaic glass maintains low reflectance. The alteration in the propagation path of the incident light, coupled with the internal reflection at the glass/air interface, allows some light to undergo multiple refractions and reflections within the photovoltaic glass (as illustrated in Fig. 1(c)), achieving a substantial lateral propagation distance. Such lateral propagation enables the light to circumvent obstructions on the photovoltaic glass, reaching the area beneath these obstructions. The model of bubble-containing photovoltaic glass is illustrated in Fig. 1(d). Here, the glass has a side length of 20 cm and a thickness of 3.2 mm, and the bubbles are positioned symmetrically at the center of the glass surfaces.

Next, we utilized the Monte Carlo ray-tracing method to investigate the haze of the bubble-containing photovoltaic glass and its correlation with the distribution, diameter, and surface density of the bubbles. We employed a grid light source with an area of $20 \times 20 \text{ cm}^2$ and a ray beam surface density of 2025 cm^{-2} , setting the ray-tracing threshold at 5×10^{-4} .

2.2. Model of the photovoltaic module with a single cell shaded

To assess the ability of incident light to circumvent obstruction when using the bubble-containing photovoltaic glass, we placed a $6.6 \times 6.6 \text{ cm}^2$ obstruction at the central position above a $20 \times 20 \text{ cm}^2$ photovoltaic glass, as depicted in Fig. 2(a). Employing the Monte Carlo ray-tracing method, we computed the flux of light at the back surface of the glass beneath the obstruction. Furthermore, we explored the relationship between light flux and factors such as bubble distribution, size, and surface density, in the bubble-containing glass. The upper surface of the obstruction was set to be a perfect absorber of light. The light source configuration remained consistent with the aforementioned setup.

It's important to note that the light flux provided by the ray-tracing method encompasses all rays that "arrive" at the surface. Hence, it includes an additional amount brought about by multiple internal reflections within the glass, as illustrated in Fig. 2(c). To eliminate this additional amount, we devised a strategy as follows. In the first step, we quantified the light flux (F_a) at the back surface of the glass. This flux comprises the transmitted light (T), the light unable to pass through the glass (denoted as ①, equivalent to light that undergoes a single reflection), and the additional light flux resulting from multiple reflections (denoted as ②, ③, ...). In the second step, we set the back surface of the glass as a perfect absorber and calculated its absorbed light flux (F_b). This flux only encompasses the transmitted light T and light that undergoes a single reflection ① (referring to the amount without the perfect absorber being set). Hence, the additional amount in the light flux registered at the back surface of the glass can be expressed as

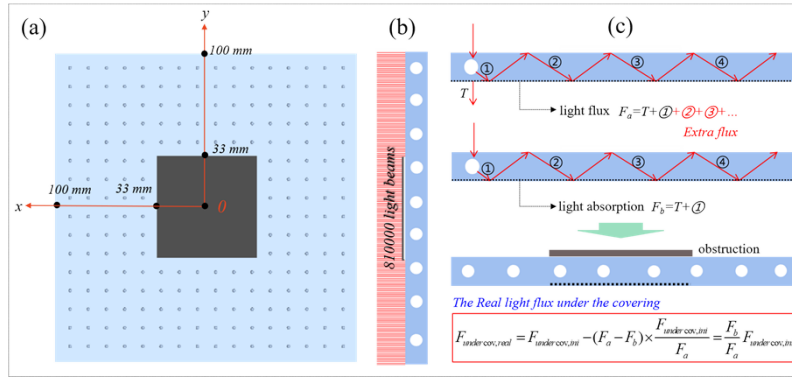


Fig. 2. Schematic representation of the bubble-containing photovoltaic glass and obstruction: (a) front view of the model, (b) side view of the model; and (c) method for calculating the light flux under the obstruction.

$F_a - F_b$. Given that the magnitude of $F_a - F_b$ is expected to be approximately proportional to the total light flux, the additional light flux in the shaded area can be estimated using the following formula:

$$\begin{aligned} \Delta F_{cov} &= (F_a - F_b)_{glass, without-cov} \times \frac{A_{cov}}{A_{glass}} \times \frac{F_{cov, cal}/A_{cov}}{F_a/A_{glass}} \\ &= (F_a - F_b)_{glass, without-cov} \times \frac{F_{cov, cal}}{F_a} \end{aligned} \quad (1)$$

Here, ΔF_{cov} represents the additional light flux beneath the covered region, A_{cov} denotes the area of the covered region, A_{glass} signifies the area of the glass, and $F_{cov, cal}$ represents the directly computed light flux beneath the covered region. Applying this equation allows for an estimation of the actual light flux beneath the covered region:

$$F_{cov, act} = F_{cov, int} - \Delta F_{cov} = \frac{F_b}{F_a} F_{cov, cal} \quad (2)$$

To estimate the effect of using this bubble-containing glass on enhancing the output power of a photovoltaic module in the presence of obstruction and reducing the reverse bias voltage on the shaded cell, we applied it to a 72×2 series-parallel connected photovoltaic module using Matlab/Simulink. The performance parameters of the solar cells under standard test conditions were set as $V_{oc} = 0.6938$ V, $I_{sc} = 7.0250$ A, $V_{mp} = 0.5847$ V, $I_{mp} = 6.5950$ A, and $FF = 79.10\%$. One cell within the module is completely covered. The output characteristics of the module under scenarios using regular and bubble-containing photovoltaic glass were compared.

3. Results and discussions

3.1. Haze of the bubble-containing photovoltaic glass

Haze is defined as the percentage of the scattered light flux, T_2 , deviating more than 2.5° from the incident direction, in relation to the total light flux transmitted through a transparent object, T_1 , when a beam of parallel light is vertically projected onto it. Therefore, high haze implies that a greater amount of incident light is scattered at large angles.

The actual haze was calculated using the following method, as illustrated in Fig. 3(a). The first step involved placing a square receiver, A_1 , behind the bubble-containing glass to obtain the total light flux, T_1 , transmitted through the glass. In the second step, after removing receiver A_1 , a convex lens was positioned behind the glass. At the focal point of the convex lens (the focal length $f = 974$ mm), a circular receiver, A_2 , with a radius of 50 mm was placed to precisely

capture the scattered light flux, T_2 , deviating within 2.5° from the incident direction, as depicted in Fig. 3(b). Thus, the haze of the bubble-containing glass can be calculated as follows:

$$H = (T_1 - T_2)/T_1 \quad (3)$$

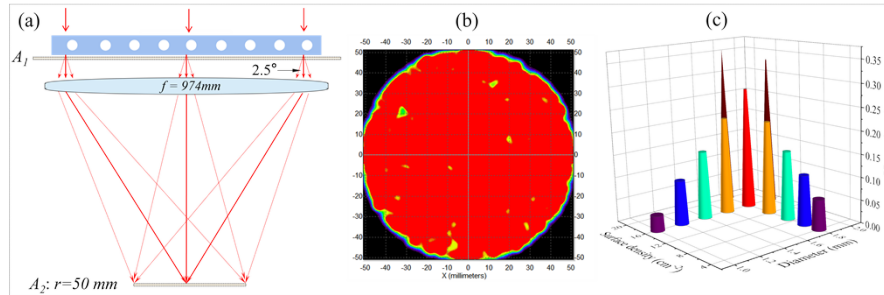


Fig. 3. (a) Schematic illustrating the calculation method of haze, (b) Image depicting the light distribution on the circular acceptor A_2 , and (c) Relationship between haze and bubble diameter and surface density.

Here, we explored the relationship between the haze of bubble-containing photovoltaic glass concerning the distribution, diameter, and surface density of the bubbles. For bubbles with a diameter of 1.8 mm and a surface density of 16 cm^{-2} , the glass exhibited hazes of 27.23% and 27.21% under uniform and random distributions, respectively. It is noteworthy that in the case of uniformly distributed bubbles, the relative positioning of an obstruction on the photovoltaic glass significantly influences the glass's capability to allow light to circumvent the obstruction. Therefore, in the subsequent simulations, we opted for a random distribution of bubbles within the glass.

The relationship between the haze of photovoltaic glass and the diameter of bubbles, with surface density fixed at 16 cm^{-2} , as well as the relationship between the haze of photovoltaic glass and the surface density of bubbles, with diameter fixed at 1.8 mm, are depicted in Fig. 3(c). Evidently, the haze of the photovoltaic glass increases with an increase in bubble size and density. However, a higher haze does not necessarily imply a stronger ability of incident light to circumvent large-sized obstruction on the photovoltaic glass. This is because excessively large bubble diameter and high surface density can increase the number of scattering events for the laterally propagating light, as depicted in Fig. 1(b). Paradoxically, this might potentially reduce the capability of incident light to circumvent large-sized obstruction.

3.2. Capability of light to circumvent obstruction when utilizing bubble-containing photovoltaic glass

To explore the impact of bubble diameter and surface density on the ability of incident light to circumvent a large-sized obstruction on the photovoltaic glass, we initially calculated the light intensity at each point at the back surface of the glass beneath the obstruction, following Eq. (2). Subsequently, we determined the average light intensity within the covered area by integrating the light intensity at each point across the entire covered area and dividing it by the area of the covered region. The results are depicted in Fig. 4.

Evidently, the ability of incident light to bypass a large-sized obstruction on the photovoltaic glass does not increase in tandem with the haze as the bubble size and surface density increase. From Fig. 4(a), it can be observed that as the bubble diameter increases, the ability of incident light to circumvent large-sized obstruction displays a trend of initial increase, followed by decrease, subsequent increase, and then decrease again. Moreover, this trend is independent of the bubble

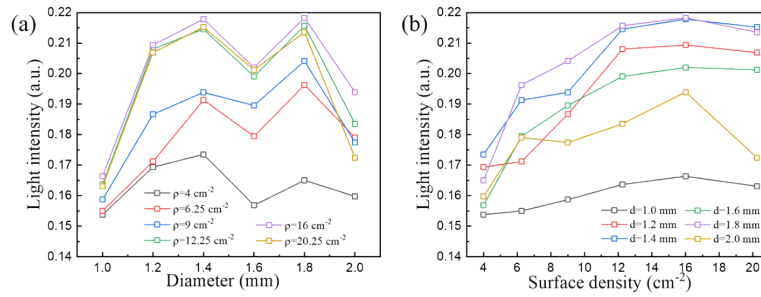


Fig. 4. Relationship between the average light intensity under the obstruction and the bubble (a) diameter and (b) surface density.

surface density. This behavior can be reasonably attributed to the significant influence of the distance between the bubbles and the upper and lower surfaces of the glass on the light-scattering angles of individual bubbles. When the bubble sizes are 1.4 mm and 1.8 mm, the proportion of light undergoing large-angle scattering is the highest, indicating the strongest lateral light propagating within the glass.

In Fig. 4(b), it is evident that with an increase in bubble surface density, the ability of incident light to bypass large-sized obstruction exhibits a trend of initial increase followed by a decrease. This phenomenon occurs because light scattered at large angles by individual bubbles experiences further scattering due to adjacent bubbles. As the bubble density increases, the total amount of light subjected to large-angle scattering increases; however, simultaneously, the number of times the lateral propagating light is scattered also increases. There exists an optimal bubble surface density of 16 cm^{-2} that strikes a balance between these two effects. At this bubble surface density, the incident light achieves the best capability to bypass obstructions.

Taking into account the combined influence of bubble diameter and surface density, the optimal condition for incident light to circumvent obstruction occurs with a bubble diameter of 1.8 mm and a surface density of 16 cm^{-2} . In this scenario, for a $20 \times 20 \text{ cm}^2$ photovoltaic glass, the average light intensity underneath a $6.6 \times 6.6 \text{ cm}^2$ obstruction can reach 21.83% of the incident light intensity. The spatial distribution of transmitted light through the bubble-containing photovoltaic glass in the absence of obstruction and with obstruction are illustrated in Figs. 5(a) and 5(b), respectively.

In Fig. 5(a), it can be observed that the existence of bubbles increases the reflectance of the photovoltaic glass to 14.7%, notably higher than the value of 6.3% without bubbles. This increase can be attributed to the large-angle scattered light caused by the bubbles, which contributes to the augmented light escaping from the glass's upper surface. Such elevated reflectance can be mitigated by introducing anti-reflection structures on the upper surface of the glass [26], a consideration we will explore in our forthcoming studies.

From Fig. 5(b), it's visually evident that there is a significant light flux in the shaded area. Despite a gradual attenuation of light intensity from the peripheral regions towards the center within the shaded area, the central region maintains a relatively stable and substantial light intensity, reaching up to 11.6% of the incident light. This indicates that the presence of bubbles indeed allows certain rays to maintain a long lateral propagation distance, thereby circumventing the obstruction to reach the area beneath it.

3.3. Effect of enhanced output power using bubble-containing photovoltaic glass

Here, we have applied the bubble-containing photovoltaic glass to a 72×2 series-parallel connected photovoltaic module and evaluated the effect of using this photovoltaic glass on enhancing the short-circuit current, maximum power output, and reducing the reverse bias voltage

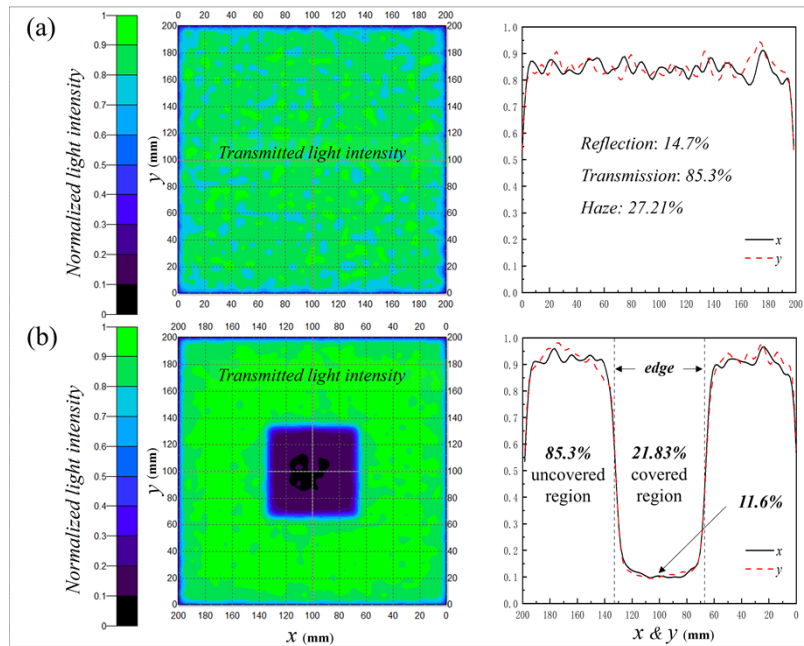


Fig. 5. Transmission light distribution of the bubble-containing photovoltaic glass (a) in the absence of obstruction and (b) with obstruction. The percentages represent the ratio to the incident light intensity.

on the shaded cell. As illustrated in Fig. 6(a), one cell within the module is completely covered. The incident irradiance on the covered and uncovered cells was set based on the previously obtained calculation results, which are given in Fig. 6(b).

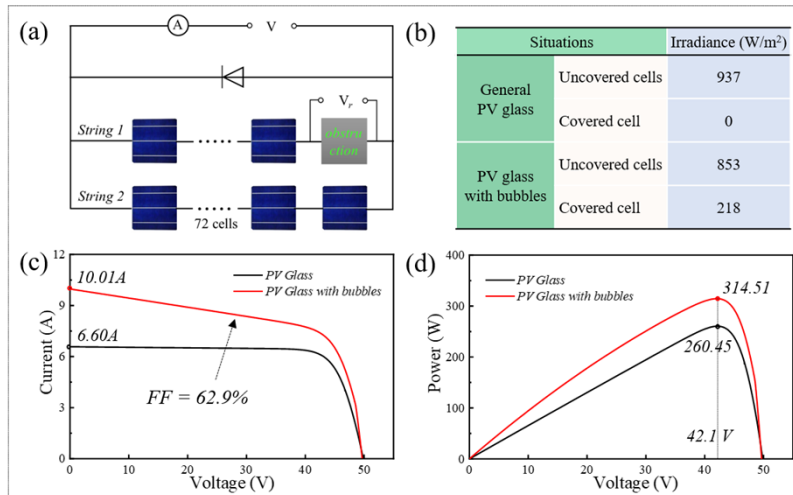


Fig. 6. (a) Illustration of a 72 × 2 series-parallel connected photovoltaic module with a single cell shaded; (b) Irradiance settings utilized in the Simulink simulations. The (c) IV and (d) PV curves of the photovoltaic module comparing outcomes using the regular photovoltaic Glass and bubble-containing photovoltaic Glass.

When using the bubble-containing photovoltaic glass, the shaded cell can receive an irradiance of 218 W/m^2 , thereby possessing a certain power generation capability. Therefore, the use of bubble-containing photovoltaic glass elevates the short-circuit current of the photovoltaic module from 6.6 A to 10.01 A , indicating a substantial increase of 51.7% , as illustrated in Fig. 6(c). However, this short-circuit current, 10.01 A , is significantly lower than the 11.98 A obtained without shading, signifying that shading effectively introduces a series resistance in string 1. This equivalent series resistance leads to a substantial decrease in the fill factor of the entire module, dropping from 79.1% to 62.9% . Hence, the enhancement in the maximum power output of the module is not as pronounced as the increase in the short-circuit current. As depicted in Fig. 6(d), utilizing bubble-containing photovoltaic glass enhances the module's maximum output power from 260.45 W to 314.51 W , representing an improvement of 20.8% .

Additionally, when the photovoltaic module is at its maximum power point, utilizing bubble-containing glass results in a reverse bias voltage of 5.6 V on the shaded cell, whereas with regular glass, the reverse bias voltage on the shaded cell is 7.0 V . This indicates that the increase in output current from the shaded cell can also diminish the reverse bias voltage applied by other cells onto the shaded one. This reduced reverse bias voltage can effectively suppress the generation of hotspots, safeguarding the shaded cell.

4. Conclusions

To enhance the output capability of photovoltaic modules under partial shading and effectively mitigate hotspot effects, in this study, we have devised a novel photovoltaic glass by introducing a layer of bubbles into the conventional photovoltaic glass. The introduced bubbles not only alter the path of incident light, thereby increasing the glass's haze; but also enable the redirected light rays to exhibit extended lateral propagation within the photovoltaic glass, which enables incident light to circumvent large-sized obstructions.

Based on ray-tracing simulations, it is found that the haze of bubble-containing photovoltaic glass increases with the diameter and surface density of the bubbles. However, excessively large bubble diameter and high surface density increase the number of scattering events for the laterally propagating light. Therefore, larger diameters or higher surface densities do not necessarily result in a stronger ability for incident light to circumvent large-sized obstruction on the photovoltaic glass. We have investigated the impact of bubble diameter and surface density on the ability of incident light to circumvent a $6.6 \times 6.6 \text{ cm}^2$ obstruction on the photovoltaic glass. The results showed that as the bubble diameter increased, the capacity of incident light to circumvent the obstruction exhibited a trend of increasing-decreasing-increasing-decreasing; Notably, this trend was independent of bubble surface density. This behavior can be attributed to the significant influence of the distance between the bubbles and the upper and lower surfaces of the glass on the light scattering angle of individual bubbles. With an increase in bubble surface density, the ability of incident light to circumvent the obstruction exhibited a trend of initially increasing and subsequently decreasing. This is because as the bubble surface density increases, the total amount of light scattered at large angles by the bubbles increases; however, simultaneously, the number of times the laterally propagating light is scattered also increases. There exists an optimal bubble surface density where the trade-off between these two effects is maximized.

Considering the combined influence of bubble diameter and surface density, when the bubble diameter is 1.8 mm and the surface density is 16 cm^{-2} , the incident light performs most effectively in circumventing the obstruction. In this scenario, for a $20 \times 20 \text{ cm}^2$ photovoltaic glass, the average light intensity underneath a $6.6 \times 6.6 \text{ cm}^2$ obstruction can reach 21.83% of the incident light intensity. Applying this photovoltaic glass, which incorporates a layer of bubbles, to a 72×2 series-parallel connected photovoltaic module with one cell completely shaded, results in a notable enhancement in the module's performance. The short-circuit current of the photovoltaic module increases from 6.60 A to 10.01 A , marking a 51.7% increment; the output power rises

from 260.45 W to 314.51 W, indicating an increase of 20.8%. Furthermore, it reduces the reverse bias voltage on the shaded cell from 7.0 V to 5.6 V, which can effectively suppress the hotspot effect. This study holds significant theoretical and practical value in enhancing the actual output capacity of photovoltaic modules under shading conditions and in suppressing hotspot formation.

Funding. National Natural Science Foundation of China (51972110, 52072121, 52102245, 52232008); Beijing Municipal Natural Science Foundation (2222076, 2222077); China Three Gorges Corporation (WWKY-2021-0173); Science and Technology Commission of the Ministry of Education (2022 Strategic Research Key Project); Huaneng Group Headquarters Science and Technology Project (HNKJ20-H88).

Disclosures. The authors declare no conflicts of interest.

Data availability. No data were generated or analyzed in the presented research.

References

1. J. Zhong, W. Zhang, O. Zhao, *et al.*, "Development and challenges of bifacial photovoltaic technology and application in buildings: A review," *Renewable Sustainable Energy Rev.* **187**, 113706 (2023).
2. K. Zhou, F. Gao, J. Liu, *et al.*, "Cloud-edge collaborated dust deposition degree monitoring for distributed photovoltaic systems," *Int. J. Electr. Power Energy Syst.* **153**, 109298 (2023).
3. K. Hu, S. Cao, L. Wang, *et al.*, "A new ultra-short-term photovoltaic power prediction model based on ground-based cloud images," *J. Cleaner Prod.* **200**, 731–745 (2018).
4. J. K. Kaldellis and P. Fragos, "Ash deposition impact on the energy performance of photovoltaic generators," *J. Cleaner Prod.* **19**(4), 311–317 (2011).
5. T. Ma, Z. Guo, L. Shen, *et al.*, "Performance modelling of photovoltaic modules under actual operating conditions considering loss mechanism and energy distribution," *Appl. Energy* **298**, 117205 (2021).
6. K. Ganesan, D. P. Winston, J. J. D. Nesamalar, *et al.*, "Output power enhancement of a bifacial solar photovoltaic with upside down installation during module defects," *Appl. Energy* **353**, 122070 (2024).
7. B. Ye, J. Qi, Y. Li, *et al.*, "Research on PV array output characteristics based on shadow image recognition," in *2017 IEEE Conference on Energy Internet and Energy System Integration (EI2)*, (2017), 1–6.
8. K. Osmani, A. Haddad, T. Lemenand, *et al.*, "A critical review of PV systems' faults with the relevant detection methods," *Energy Nexus* **12**, 100257 (2023).
9. G. Trzmiel, D. Gluchy, and D. Kurz, "The impact of shading on the exploitation of photovoltaic installations," *Renewable Energy* **153**, 480–498 (2020).
10. J. Bai, Y. Cao, Y. Hao, *et al.*, "Characteristic output of PV systems under partial shading or mismatch conditions," *Sol. Energy* **112**, 41–54 (2015).
11. K. A. Kim and P. T. Krein, "Hot spotting and second breakdown effects on reverse I-V characteristics for mono-crystalline Si Photovoltaics," in *2013 IEEE Energy Conversion Congress and Exposition*, (2013), 1007–1014.
12. P. R. Satpathy and R. Sharma, "Parametric indicators for partial shading and fault prediction in photovoltaic arrays with various interconnection topologies," *Energy Convers. Manage.* **219**, 113018 (2020).
13. D. Pera, J. A. Silva, S. Costa, *et al.*, "Investigating the impact of solar cells partial shading on photovoltaic modules by thermography," in *2017 IEEE 44th Photovoltaic Specialist Conference (PVSC)*, (2017), 1979–1983.
14. I. Marinić-Kragić, F. G. Čabo, M. Jurčević, *et al.*, "Mitigation of hot-spot effect via back side cooling techniques: A potential for electrical and thermal performance improvement," *Energy and Buildings* **288**, 113010 (2023).
15. W. Lu, Z. Liu, J. F. Flor, *et al.*, "Investigation on designed fins-enhanced phase change materials system for thermal management of a novel building integrated concentrating PV," *Appl. Energy* **225**, 696–709 (2018).
16. C. Wu, D. Q. Zhou, Z. H. Li, *et al.*, "Hot spot detection and fuzzy optimization control method of PV module," *Proceedings of the CSEE* **33**, 50–61 (2013).
17. L. Liu, H. Qian, E. Sun, *et al.*, "Power reduction mechanism of dust-deposited photovoltaic modules: An experimental study," *J. Cleaner Prod.* **378**, 134518 (2022).
18. H. Yang, W. Xu, H. Wang, *et al.*, "Investigation of reverse current for crystalline silicon solar cells—New concept for a test standard about the reverse current," in *2010 35th IEEE Photovoltaic Specialists Conference*, (2010), 2806–2810.
19. A. Wang and Y. Xuan, "Close examination of localized hot spots within photovoltaic modules," *Energy Convers. Manage.* **234**, 113959 (2021).
20. H. Park and D. Kim, "Influence on the haze effect of Si thin-film solar cell on multi-surface textures of periodic honeycomb glass," *Trans. Electr. Electron. Mater.* **22**(1), 80–90 (2021).
21. L. Chen, Y. Huang, Z. Qian, *et al.*, "A novel mask technology of glass HF etching and application in photovoltaic cells," *J. Alloys Compd.* **783**, 428–433 (2019).
22. Y. M. Song, Y. Jeong, C. I. Yeo, *et al.*, "Enhanced power generation in concentrated photovoltaics using broadband antireflective coverglasses with moth eye structures," *Opt. Express* **20**(S6), A916–A923 (2012).
23. J.-H. Kim, J. W. Cho, I. Jeon, *et al.*, "Synergistically designed antireflective cover for improving wide-angle photovoltaic efficiencies," *Opt. Express* **30**(23), 42406–42414 (2022).
24. M. A. Tsai, H. W. Han, Y. L. Tsai, *et al.*, "Embedded biomimetic nanostructures for enhanced optical absorption in thin-film solar cells," *Opt. Express* **19**(S4), A757–A762 (2011).

25. Z. Zhou, Y. Jiang, N. Ekins-Daukes, *et al.*, "Optical and thermal emission benefits of differently textured glass for photovoltaic modules," *IEEE J. Photovoltaics* **11**(1), 131–137 (2021).
26. S. Ahn, H. Park, J. Cho, *et al.*, "Reactive-ion-etched glass surface with 2D periodic surface texture for application in solar cells," *Optik* **229**, 166304 (2021).